INT. J. NUM. METH. HEAT FLUID FLOW, VOL. 5, 717–733 (1995)

NUMERICAL LAMINAR AND TURBULENT FLUID FLOW AND HEAT TRANSFER PREDICTIONS IN TUBE BANKS

FRANZ ZDRAVISTCH†, CLIVE A. FLETCHER† AND MASUD BEHNIA‡

† *Centre for Advanced Numerical Computation in Engineering and Science (CANCES), University of New South Wales, Sydney, NSW 2052, Australia*

‡ *School of Mechanical and Manufacturing Engineering, University of New South Wales, Sydney, NSW 2052, Australia*

ABSTRACT

Numerical predictions of laminar and turbulent fluid flow and heat transfer around staggered and in-line tube banks are shown to agree closely with seven experimental test cases. The steady state Reynolds-averaged Navier-Stokes equations are discretised by means of a cell-centred finite-volume algorithm. Two-dimensional results include velocity vectors and streamlines, surface shear stresses, pressure coefficient distributions, temperature contours, local Nusselt number distributions and average convective heat transfer coefficients, and indicate very good agreement with experimental data. It is found that a relatively fine grid is required to be able to predict the surface heat transfer behaviour accurately. Also, three-dimensional simulations are shown, which are physically consistent. The numerical procedure presented here is robust, accurate and time efficient, making it suitable as a design tool for tube banks in heat exchangers.

KEY WORDS Tube banks Finite volume method Convective heat transfer Tube bundles Crossflow Heat exchangers

INTRODUCTION

Heat exchangers containing tube banks in crossflow are widely used in industrial and power engineering applications. The local fluid flow and heat transfer around a tube in a tube bank is complex, and it depends primarily on the inlet flow conditions, turbulence intensity, surface roughness and the geometry of the tube bank[1]. Traditionally, tube bank design has been mostly carried out by experimental and/or empirical methods. Experiments usually involve high costs (economic and temporal) and sometimes technical difficulties in obtaining direct full-scale measurements, and empirical methods do not permit the analysis of the local fluid flow and heat transfer characteristics within the tube bank. This motivates the use of computational fluid dynamics (CFD) codes[2] as an alternative design tool for tube bank heat exchangers.

Numerical solutions provide the values of the dependent variables throughout the computational domain, allowing a more detailed comprehension of the phenomena involved. Several fluid flow and heat transfer simulations in tube banks have been reported, which are either finite difference[3,4] or finite element[5] based, and focus on either laminar[3,4,5] or turbulent[6] flows. Finite difference and finite element algorithms present some disadvantages.

The former approach often requires a restriction on the complexity of the geometric domain to achieve sufficient accuracy and the judicious use of artificial dissipation to ensure robustness.

0961–5539/95/080717–17$2.00

Received January 1994
Revised August 1994

The latter often leads to computationally expensive algorithms, making the codes less suitable for design purposes. In contrast, the finite volume formulation exploits the economy of finite difference discretisation and the geometric flexibility of finite element methodology. Faghri and Rao[7] used a finite volume formulation to predict two-dimensional flow and heat transfer in finned and unfinned tube banks for the laminar regime.

The contribution of the present study is two-fold. First, a finite volume formulation is developed which is capable of simulating both laminar and turbulent flow and heat transfer around staggered and in-line tube banks, with sufficient robustness and efficiency so that the code can be used as a design tool for tube bank heat exchangers. Second, a comprehensive validation of the results is undertaken, including local heat transfer, against available experimental data over a wide range of Reynolds numbers.

It may be suggested that the various test cases simulated in this paper could be considered as a 'standard' set of test cases that all industrial CFD codes should be assessed against. This would provide a partial assurance of quality.

Also, three-dimensional computations around tube bank configurations between two parallel plates (longitudinal fins) are presented, which are verified for physical consistency. Although no detailed experimental data are available for these test cases, this is the real situation for which the design use of CFD codes must be effective.

THEORETICAL FORMULATION

Here, the appropriate governing equations and boundary conditions are indicated and discussed. Since the present formulation is to be used in a design mode, a two-layer wall function is introduced to represent accurately the near-wall behaviour without compromising the overall economy of execution.

Governing equations

The flow and heat transfer around tube bank configurations can be accurately described by the steady-state Reynolds-averaged Navier-Stokes equations. The assumption of steady-state flow is consistent for tube banks in crossflow, since the constraining effect of the neighbouring tubes suppresses the appearance of vortex shedding, even for high Reynolds numbers. These equations, retaining only dominant terms, can be written as:

$$\frac{\partial}{\partial x_i}(\rho u_i) = 0 \tag{1}$$

$$\frac{\partial}{\partial x_i}(\rho u_i u_j + \delta_{ij} p_j - \tau_{ij} + \rho \overline{u_i' u_j'}) = 0 \tag{2}$$

$$\frac{\partial}{\partial x_i}\left(\rho C_p u_i T - k_{\text{eff}} \frac{\partial T}{\partial x_i}\right) = u_i \frac{\partial p}{\partial x_i} \tag{3}$$

Here, the standard nomenclature found in the literature is used[2]. The term k_{eff} is the effective thermal diffusivity, which includes the eddy diffusivity, and accounts for the conductive heat transfer exchange in laminar or turbulent regimes. Equations (2) contain Reynolds stresses that are modelled by the standard k–ε turbulence model. The following transport equations govern the behaviour of k and ε:

$$\frac{D\varepsilon}{Dt} = \frac{1}{\rho}\frac{\partial}{\partial x_k}\left[\frac{\mu_t}{\sigma_e}\frac{\partial \varepsilon}{\partial x_k}\right] + \frac{C_1 \mu_t}{\rho}\frac{\varepsilon}{k}\left(\frac{\partial U_i}{\partial x_k} + \frac{\partial U_k}{\partial x_i}\right)\frac{\partial U_i}{\partial x_k} - C_2 \frac{\varepsilon^2}{k} \tag{4}$$

$$\frac{Dk}{Dt}=\frac{1}{\rho}\frac{\partial}{\partial x_k}\left[\frac{\mu_t}{\sigma_e}\frac{\partial k}{\partial x_k}\right]+\frac{\mu_t}{\rho}\left(\frac{\partial U_i}{\partial x_k}+\frac{\partial U_k}{\partial x_i}\right)\frac{\partial U_i}{\partial x_k}-\varepsilon \tag{5}$$

Details of the k–ε turbulence model and the appropriate values for the parameters and constants can be found elsewhere[8].

Boundary conditions

The solution domain is defined to take advantage of the symmetry conditions of the flow, which are valid assuming that the number of tube rows (m) and columns (n) is large (m, $n > 10$). This is certainly the case for practical applications. The boundaries of the computational domain for an in-line tube bank configuration are presented in *Figure 1*. Four types of boundary conditions are implemented:

Inlet plane: Dirichlet boundary conditions are imposed at the inlet boundary.
Outlet plane: Streamwise gradients (Neumann boundary conditions) for the variables are set to zero at the outlet plane.
Symmetry planes: On the upper and lower symmetry planes normal gradients are set to zero.
Solid surfaces: No-slip conditions and either constant wall temperature or constant heat flux are specified at the walls.

Some discussion is necessary about the boundary conditions implemented at the outflow plane. The assumption of zero streamwise gradient of the velocities and turbulent variables can be justified by the physical conditions of the flow at the outlet boundary. The region around 90° from the front stagnation point of an individual tube is located at the minimum cross section of the tube bank, where maximum velocities are present, and where the flow tends to be aligned with the streamwise direction. From the numerical point of view, when the above outflow boundary conditions are implemented and nothing is specified about the pressure, the continuity equation may not be satisfied over the computational domain[9]. In this case, any discrepancies in mass conservation are corrected by adding a constant to the streamwise velocity at the outlet plane. The velocity increment is calculated by dividing the difference in mass flow between the inlet and the outlet planes by the number of outflow control volumes.

Another alternative is the use of periodic boundary conditions. They are physically consistent only downstream of the seventh row in the tube bank, where periodicity of the flow is achieved. This option limits the simulation only to fully developed flow conditions, which is not the case for the first tubes in the bank, where important changes in flow and heat transfer take place.

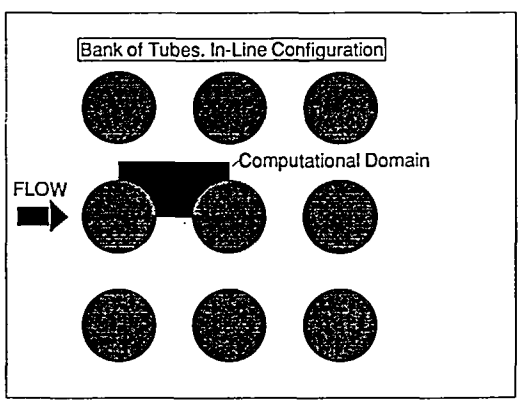

Figure 1

A two-layer wall function[10], which assumes that two distinguishable fluid layers (viscous sublayer and fully turbulent wall dominated layer) are present, is used to relate the solid surface boundary conditions to the first grid point away from the wall, which must be located outside the viscous sublayer ($y^+ > 11$). For laminar flow, the wall heat flux and the temperature are related by:

$$\dot{q}''_w = k \left.\frac{\partial T}{\partial n}\right|_w \tag{6}$$

where $\dot{q}''_w = k \left.\dfrac{\partial T}{\partial n}\right|_w$ is evaluated from the temperature solution.

For turbulent flow, the heat flux and the temperature at the wall are related by the following expression[11] (which exploits the dominant logarithmic form of the wall function):

$$\frac{(T_w - T_p)\rho C_p C_\mu^{1/4} k_p^{1/2}}{\dot{q}''_w} = Pr_t \left[\frac{1}{k}\ln(E y_p^+) + P\right] \tag{7}$$

where the empirical function P is given by[11]:

$$P = 9.24\left[\left(\frac{Pr}{Pr_t}\right)^{3/4} - 1\right]\left[1 + 0.28\exp\left(-0.007\frac{Pr}{Pr_t}\right)\right] \tag{8}$$

COMPUTATIONAL METHOD

A cell-centred finite volume formulation based on the use of area vectors[2] is used to achieve discrete mass conservation and to maintain reasonable accuracy as the grid is distorted. Dispersion-adjusted interpolation is introduced to model accurately the convective terms. An auxiliary potential method with SIMPLEC[2] algorithm is used to couple the velocity, pressure and density solutions.

Computational algorithm

The governing equations (1), (3) can be written symbolically as:

$$\frac{\partial F^{i'}}{\partial x_i} = S^{i'} \tag{9}$$

Equation (9) lends itself to a general finite-volume discretisation, which can be implemented directly in physical space using the concept of area vectors[2]. In this case (9) becomes, for a six-sided control-volume:

$$\sum_1^6 F_n^{i'} \cdot A_n = |J^{-1}|\langle S^{i'}\rangle \tag{10}$$

where A_n represents the area vector of the nth face, $\langle S^{i'}\rangle$ denotes the source term evaluated at the centre of the control volume, and the determinant of the inverse Jacobian $|J^{-1}|$, is the effective volume of the control volume, which can be obtained from:

$$|J^{-1}| = \tfrac{1}{3}\mathbf{A} \cdot x^{cf} \tag{11}$$

where $\mathbf{A} = |\mathbf{J}^{-1}|\mathbf{J}$, and x^{cf} is the vector of the centroids of the faces of the control volume.

Considering the transport nature of the governing equations, F^i can be written as

$$F^i = \rho u^i \psi - \mu \frac{\partial \psi}{\partial x^i} \tag{12}$$

where ψ is a general scalar, e.g. u in the x-momentum equation or T in the energy equation. Therefore, one component of the left hand side of (10) can be expressed as:

$$F_n^i \cdot A_n = \{\rho \mathbf{u} \cdot A^{(i)} \psi - \mu A^{(i)} \cdot \nabla \psi\}_n \tag{13}$$

where $\mathbf{u} \cdot A^{(i)}$ represents the normal flux through the nth surface, and μ is the total diffusion coefficient, either the total viscosity for the momentum equations or the effective thermal diffusivity in the energy equation. The second term can be evaluated in terms of either physical coordinates or generalised coordinates. The latter approach is chosen, leading to:

$$A^{(i)} \cdot \nabla \psi = \frac{A^{(i)} A^{(j)}}{|\mathbf{J}^{-1}|} \frac{\partial \psi}{\partial \xi^j} \tag{14}$$

Defining the generalised convection and diffusion coefficients as:

$$C_n^i = \{\rho \mathbf{u} \cdot A^{(i)}\}_n \tag{15}$$

$$D_n^{ij} = \mu A_n^{(i)} \cdot A_n^{(j)} / |\mathbf{J}^{-1}| \tag{16}$$

Equation (13) becomes:

$$F_n^i \cdot A_n = C_n^i \psi_n - D_n^{ij} \left[\frac{\partial \psi}{\partial \xi_j}\right]_n \tag{17}$$

The generalised convection and diffusion coefficients are evaluated at the centre of each face, whereas the dependent variables are evaluated at the centre of each control volume. This makes the evaluation of $\partial \psi / \partial \xi^j$ for derivatives normal to the face very compact. Assuming $\Delta \xi = \Delta \eta = 1$,

$$\left.\frac{\partial \psi}{\partial \xi}\right|_{i+1/2} = 0.5(\psi_{i+1,j,k} - \psi_{i,j,k}) \tag{18}$$

The first derivatives in the governing equations are evaluated using the four point asymmetric discretisation[2]. For a uniform grid, with $F^c = C^i \psi$ the value of F^c on a control surface is:

$$F_{i-1/2}^c = F_i^c + \varphi_{i-1/2}[0.5\Delta F_i - (q/3)(\Delta F_i - \Delta F_{i-1})] \tag{19}$$

Here $\varphi_{i-1/2}$ is a Roe-type limiter which can be activated if very strong gradients are expected. In the present study $\varphi_{i-1/2} = 1.0$. Also, the parameter q allows additional control over the dispersion suppression[2] properties. Here, we use $q = 0.5$, which leads to a third order accurate determination of $\dfrac{\partial F}{\partial x}$.

The discretised equations are solved sequentially at each iteration to obtain the dependent variables, using a Strongly Implicit Procedure (SIP)[2]. The solution for the velocity is denoted by $\underset{\rightarrow}{q}^*$, where $\underset{\rightarrow}{q}^T \equiv \{u, v, w\}$. To satisfy continuity it is necessary that:

$$\nabla \cdot (\rho \underset{\rightarrow}{q})^{n+1} = 0 \tag{20}$$

therefore a correction factor for the velocity is introduced:

$$\nabla \cdot (\rho \underset{\rightarrow}{q})^{n+1} = (\rho \underset{\rightarrow}{q})^* + (\rho \underset{\rightarrow}{q})^c \tag{21}$$

The correction velocity field is obtained from the velocity potential:

$$\underset{\rightarrow}{q}^c = \alpha \nabla \varphi \tag{22}$$

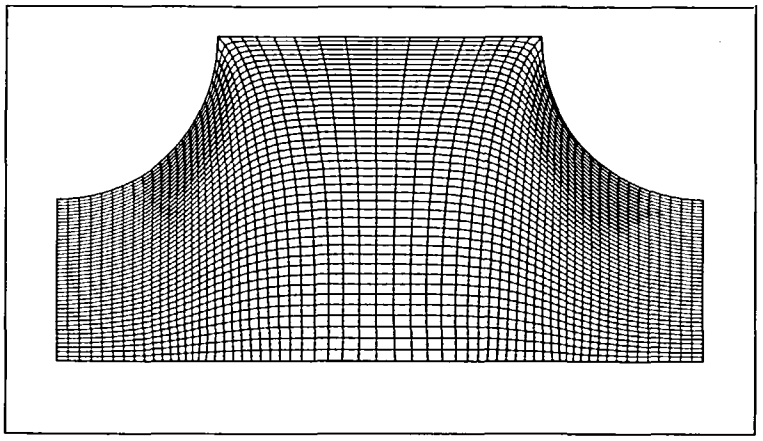

Figure 2

The pressure and density corrections can also be obtained from φ, using the auxiliary potential method[12]:

$$\rho^c = -\delta\varphi/(a^*)^2, \qquad p^c = -\beta\varphi \tag{23}$$

Here α, β and δ are under-relaxation factors and a^* is the sound speed. This leads to the following transport equation for φ:

$$\delta \frac{\partial}{\partial x_i}\left\{\frac{u_i^*\varphi}{(a^*)^2}\right\} - \alpha \frac{\partial}{\partial x_i}\left\{\rho^* \frac{\partial\varphi}{\partial x_i}\right\} \equiv \nabla\cdot(\rho q^*) - \underset{\rightarrow}{\gamma} \frac{\partial^4\varphi}{\partial\xi^{i4}} \tag{24}$$

The term $\underset{\rightarrow}{\gamma} \dfrac{\partial^4\varphi}{\partial\xi^{i4}}$ is introduced in computational space to assist in the damping of any pressure oscillations that may occur due to the fact that the discretisation algorithm is non-staggered, i.e., the velocity components and pressure are specified at the same grid points. Further description of the present formulation is available elsewhere[13].

Grid generation

The computational mesh is body-fitted, and is generated using algebraic methods[14]. Geometric stretching functions of the type $\Delta y_j = (1+\varepsilon)\Delta y_{j-1}$ are used to cluster grid points near the solid regions. The grid is smoothed via an elliptic solver for the Laplace equation using successive over-relaxation (SOR). The grid generation code allows the geometrical parameters to be set as input data. A two dimensional mesh for an in-line configuration is presented in *Figure 2* and a three dimensional grid for a staggered configuration between two parallel plates is shown in *Figure 3*.

RESULTS AND DISCUSSION

Results for realistic tube bank geometries have been obtained. Two-dimensional simulations are accurate when the influence of the surrounding walls is negligible and the flow direction is normal to the tubes longitudinal axis. This is usually the case when the tubes length to diameter ratio is greater than ten, and the number of rows (m) and columns (n) is large ($m, n > 10$)[15]. This situation is found frequently in industrial applications and laboratory experiments.

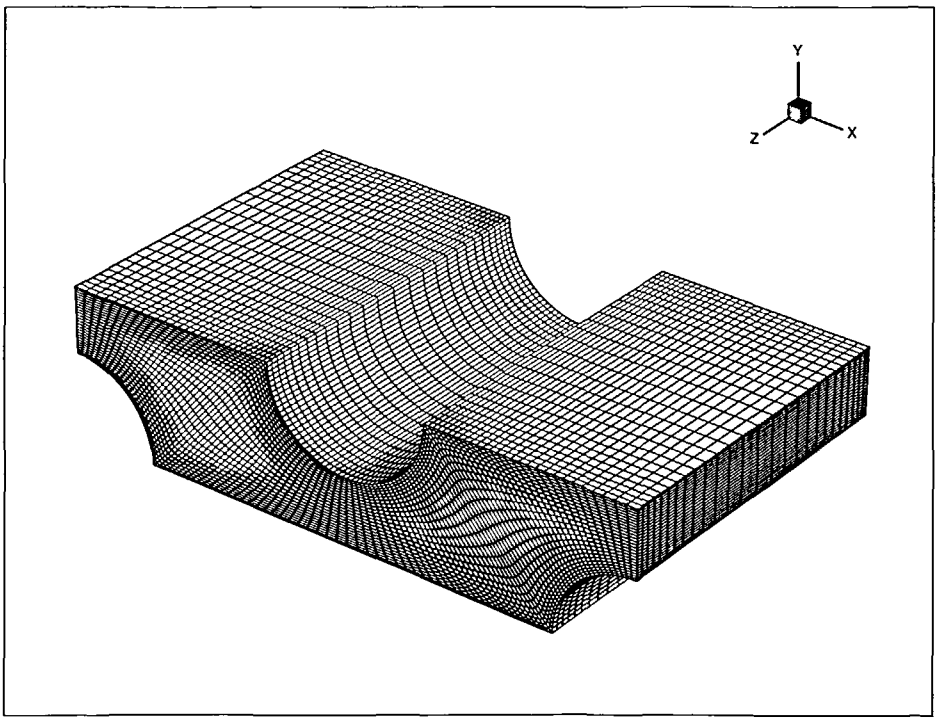

Figure 3

Three-dimensional simulations are necessary when side walls effects are important, as in tube banks with fins and/or spacers, which are mostly found in industrial heat exchangers.

Solution procedure

The strategy of computation consists of progressively simulating the flow in deeper sections in the tube bank, using the conditions at the outlet of the previous section as inlet boundary conditions for the next computational domain. This procedure is efficient, and due to the flow conditions, is also accurate, as it will be shown in *Figure 5*. A computational domain consisting of a straight section and the front half of the first cylinder is used to initiate the simulation into the tube bundle for the two-dimensional cases, and a similar geometry between two parallel surfaces is used as starting domain for the three-dimensional simulations.

Computational background

All the computations mentioned below were performed on Hewlett Packard 730 Series workstations, which have an optimal performance of about 20 MFlops. Grid sizes vary from case to case, since very fine grids are needed to accurately predict the local surface heat transfer. Also, the number of iterations required to achieve convergence is dependent on the type of flow and the Reynolds number considered. The two-dimensional isothermal laminar case (*Figure 4*) on a 65×45 grid takes 400 iterations to converge which requires 3 min of CPU time. The two-dimensional laminar case with heat transfer (*Figure 12*) on a 154×22 grid needs 1000 iterations to converge requiring 14.1 min of CPU time. The two-dimensional isothermal turbulent case (*Figure 7*) on a 134×34 grid takes 1200 iterations to converge which requires 18 min of

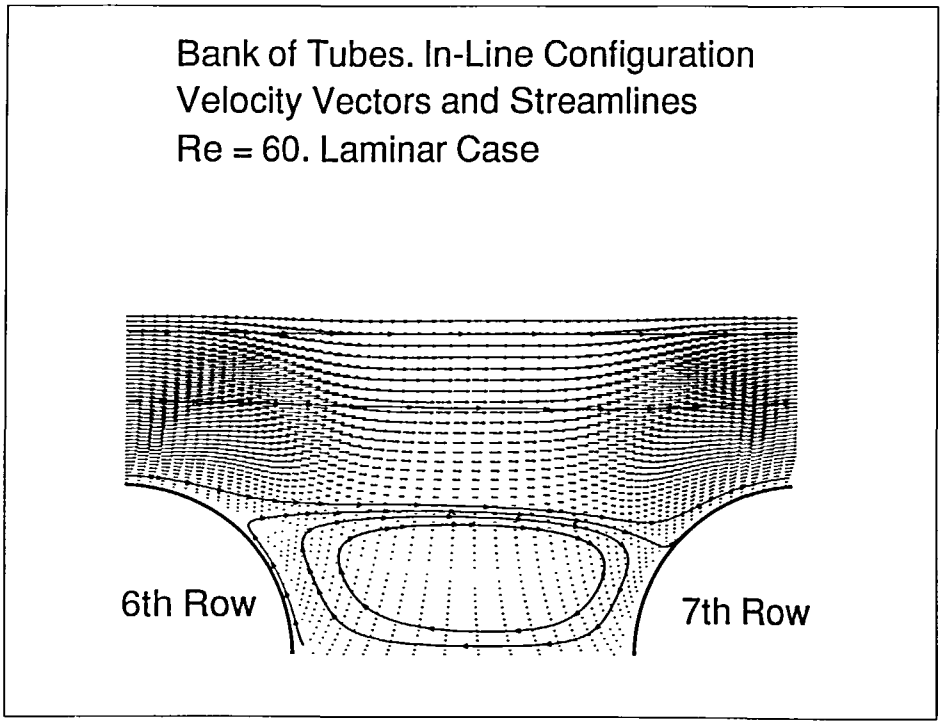

Figure 4

CPU time. For the two dimensional turbulent case with heat transfer (*Figure 14*) on a 114 × 72 grid, convergence is obtained after 1500 iterations which takes 67 min of CPU time. For the three dimensional turbulent case with heat transfer prediction (*Figure 17*), convergence is obtained after 2000 iterations, taking 10 hrs of CPU time on a 115 × 25 × 25 grid. These data show that simulations on fairly realistic geometries can be performed in reasonable CPU times.

No sufficient data has been found in the literature by the authors regarding computational costs for realistic simulations in tube bank flows with heat transfer which could permit a detailed assessment of the relative efficiency of the present code. However, Faghri and Rao[7] reported CPU times between 120 and 200 min for the flow equations, and an additional 3 to 6 min for the energy equation, when predicting a two-dimensional laminar flow using a finite-volume algorithm with a 56 × 31 grid on a NAS7000 mainframe computer using an IBM OS/MVS operating system. Also, Chang et al.[16] reported a CPU time of 20 min on a VAX 11/785 computer, when simulating a two-dimensional laminar flow with heat transfer for an in-line tube bundle using a Galerkin finite-element technique on a 324 nodes and 240 elements grid.

Two-dimensional laminar flow behaviour

Initially, laminar two-dimensional isothermal flow predictions are presented. *Figure 4* shows the typical velocity vectors and streamlines for an in-line configuration, $Re = 60$, with longitudinal pitch ratio of two ($a = 2$), and transverse pitch ratio of two ($b = 2$), between rows 6 and 7. The flow patterns are consistent with experimental visualisation data reported by Nishimura *et al.*[5]. The closed recirculation region between tubes is well captured by the simulation. It was also observed that periodicity of the flow is achieved after 7 rows inside the tube bank, which agrees with what has been reported in experimental studies.

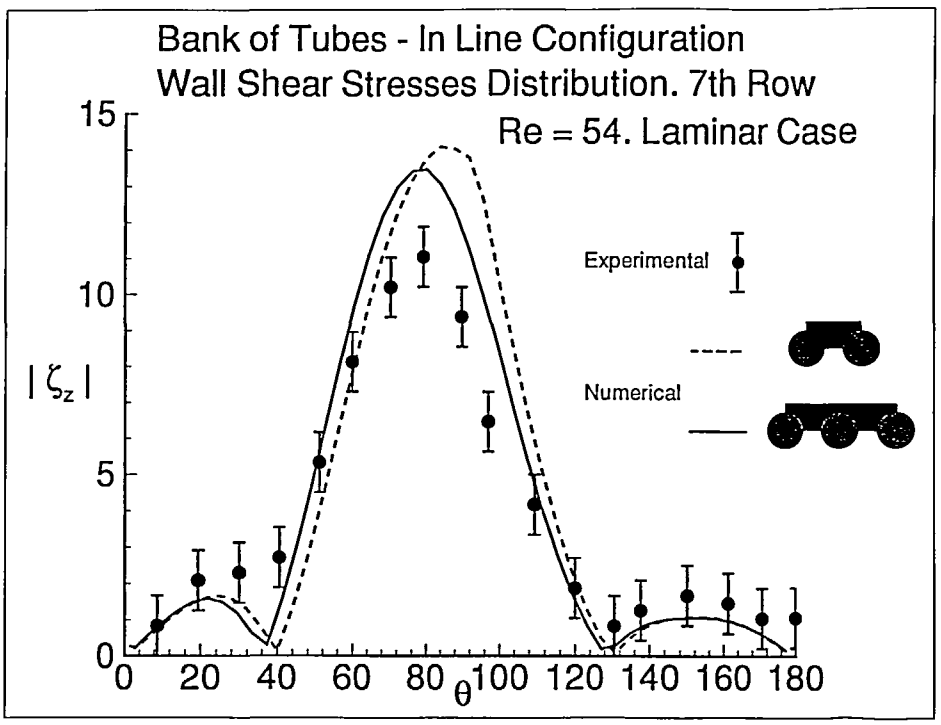

Figure 5

Figure 5 shows the dimensionless surface shear stress distribution over the seventh row for an in-line configuration, for $Re = 54$. The dashed line corresponds to the simulation on the same geometry presented in *Figure 2*, and the continuous line corresponds to a computation performed on an 'extended' geometry, in which the grid is duplicated to include the whole tube. These results indicate that the outflow boundary conditions used are realistic and that their influence is confined to the outflow region. This comparison also suggests the use of the extended geometry for in-line configurations only around the row of interest, and to advance the solution inside the tube bank using the original procedure. It is important to mention that the experimental results have a 10% to 15% uncertainty, specially in the regions of low velocity flow[5]. Nevertheless, the results show good agreement. The zero shear stress value at 40° corresponds to the reattachment point of the impinging wake from the upstream cylinder (*Figure 4*), which is not shown by experimental values. The wall shear stresses distribution over the seventh row in a staggered configuration are presented in *Figure 6*, also showing very good agreement with experimental values. Since the wall shear stress is determined from the local velocity gradient, this is a particularly demanding test case.

Two-dimensional turbulent flow behaviour

Velocity vectors and streamlines for a two-dimensional staggered configuration with $a = 2.0$ and $b = 2.0$ between rows 1 and 3 in turbulent regime at $Re = 1.5 \times 10^6$ are presented in *Figure 7*. Because of the presence of the turbulent boundary layer over the cylinder surface, the separation point is shifted downstream relative to that for laminar flow, decreasing the size of the wake. The recirculation region downstream of the first row is larger than in subsequent rows, since the turbulence intensity increases as the gas flows deeper into the tube bank, and also because the flow around the first row is more like that around an isolated tube than subsequent rows[17].

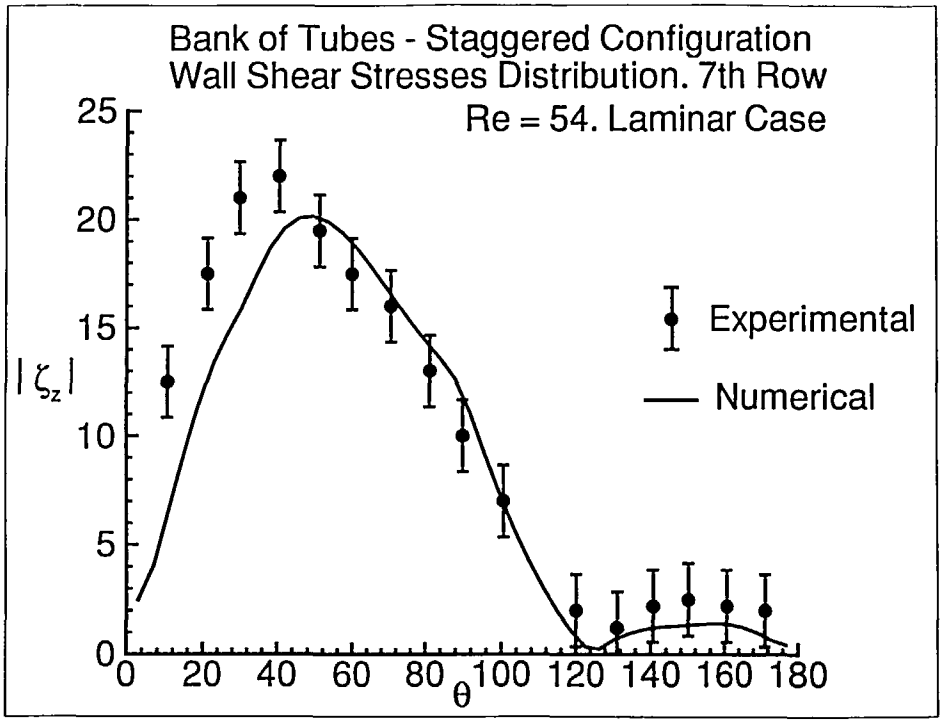

Figure 6

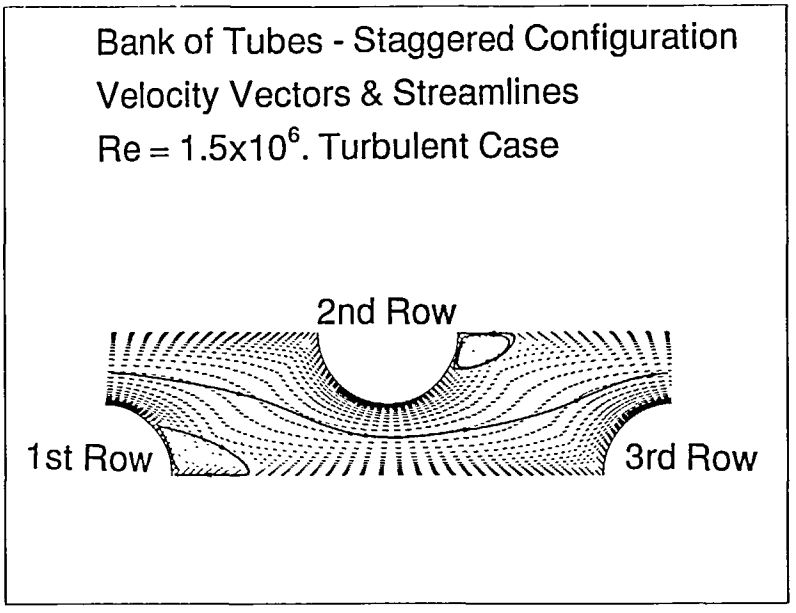

Figure 7

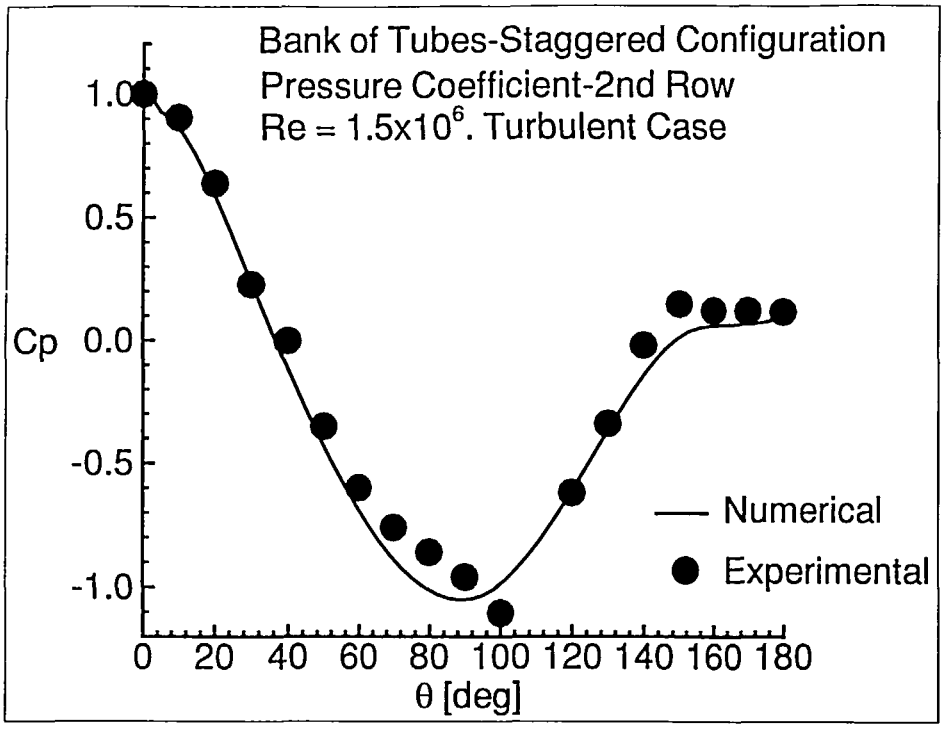

Figure 8

The pressure coefficient distribution over the second row for a staggered configuration with $a = 2.0$ and $b = 1.4$ and $Re = 1.5 \times 10^6$ is presented in *Figure 8*. The agreement with experimental results reported by Achenbach[18] is very good.

Three-dimensional flow behaviour

The streamtraces around rows one to three of a three-dimensional staggered tube bank between two parallel solid boundaries with longitudinal, transverse and side wall pitch ratios of two for laminar regime ($Re = 60$) are presented in *Figure 9*. The flow patterns are physically consistent, with the boundary layer development on the lateral solid boundaries and the presence of corner vortices created by the local boundary layer separation. This generates a region of accelerated flow towards the symmetry plane. Similar results for turbulent flow over a three-dimensional staggered configuration with $a = 1.6$, $b = 1.6$ and side walls pitch ratio of two, for $Re = 5.6 \times 10^4$, are presented in *Figure 10*. In this case, the turbulent boundary layer is able to resist the adverse pressure gradient better than the laminar boundary layer. As a result the corner vortex is weaker and there is a stronger tendency for the streamtraces to stay parallel to the side walls. Since no experimental results for this type of geometry have been found, the three-dimensional results at the symmetry plane are verified for consistency with results for similar two-dimensional configurations. These are presented in *Figure 11*. A good qualitative agreement is observed, for the side wall pitch ratio considered.

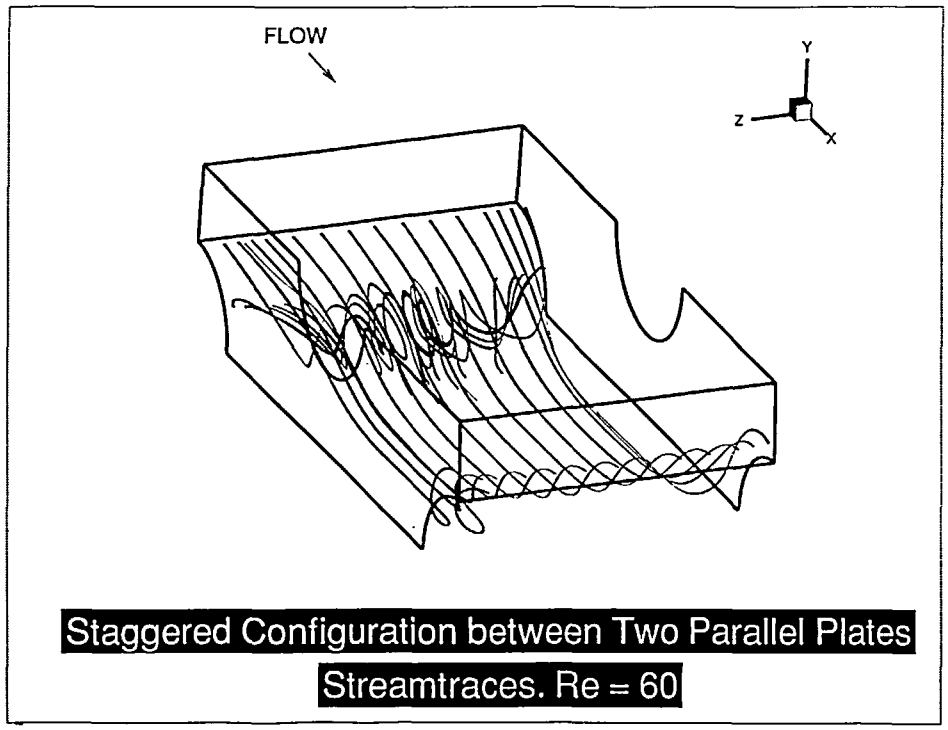

Figure 9

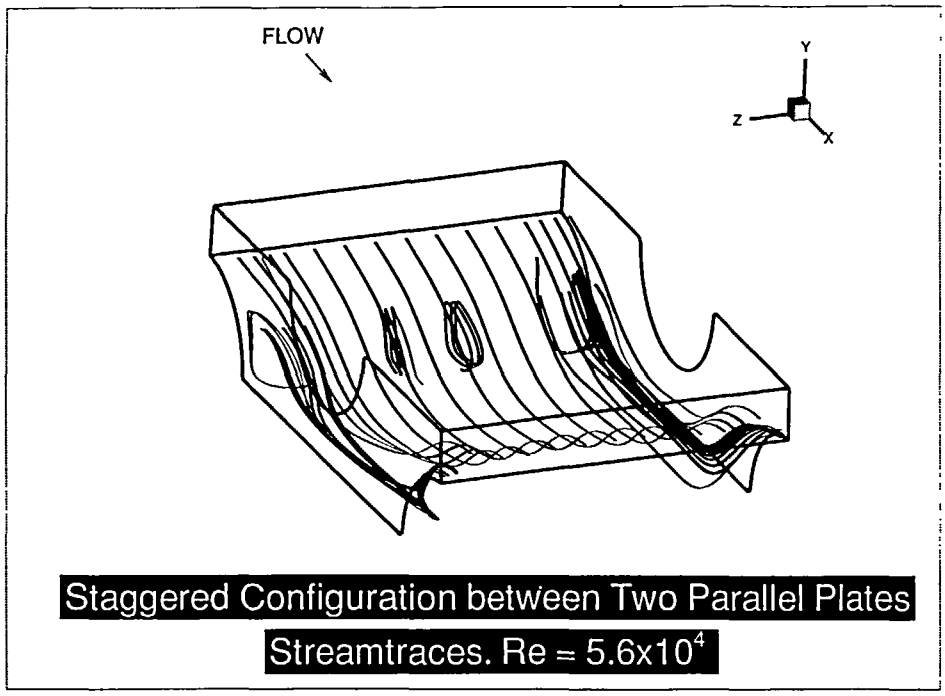

Figure 10

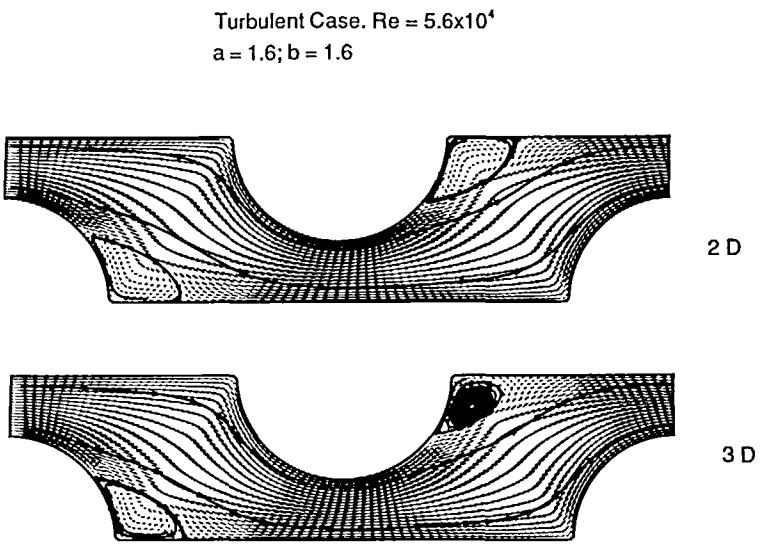

Figure 11

Heat transfer behaviour

Laminar two-dimensional heat transfer predictions around an in-line configuration with $a = 1.5$ and $b = 1.5$ are presented in *Figure 12*, for rows 1 and 2, which shows the local Nusselt number distributions for $Re = 120$ and $Pr = 0.7$. Constant temperature boundary conditions were imposed at the walls. These results agree well with other simulations[4]. The shape of the Nusselt number distribution for the first row differs from the shape over the second row, because there is no wake shading effect upstream of the first cylinder. As a result the thinner boundary layer leads to a higher temperature gradient and thus to a higher heat transfer at the wall. The minimum Nusselt number at $\theta \approx 150°$ corresponds to the boundary layer separation point, where the flow velocity is very low leading to a low temperature gradient. *Figure 13* shows the overall convective heat transfer coefficient for the same in-line configuration. In this case, the computation was repeated over ten rows, and the overall heat transfer coefficient was calculated by integrating the local heat transfer coefficient distributions in each row, and taking the average over the ten cylinders, for three different Reynolds numbers. The results show very good agreement with experimental data from Bergelin *et al.*[19]. This confirms that the solution procedure adopted in this work is also effective in computing the global heat transfer characteristics of a tube bank.

The local Nusselt distribution for the second row of a staggered tube bank with $a = 2.0$ and $b = 1.4$ for turbulent flow is presented in *Figure 14*, for $Re = 1.5 \times 10^6$ and $Pr = 0.7$, and compared with experimental results reported by Achenbach[20]. The actual boundary conditions present in the experiments are difficult to reproduce, since the experimental surface heat transfer does not occur under either constant wall temperature or constant wall heat flux. However the tubes were built of copper[20], which is a highly conductive material. In this case, it is expected that the surface heat transfer takes place in a condition close to constant wall temperature[1]. This was the wall boundary condition used for this particular simulation. Also, for the conditions of the experiment, transition effects certainly influence the local heat transfer characteristics, and cannot be accounted for by the present formulation. Nevertheless, the agreement with the experimental results is good. The minimum value of the Nusselt number distribution at the rear part of the cylinder corresponds to the separation point, which appears shifted downstream when compared with the experimental values, possibly due to unaccounted transition phenomena which affects the nature of the boundary layer and its point of separation.

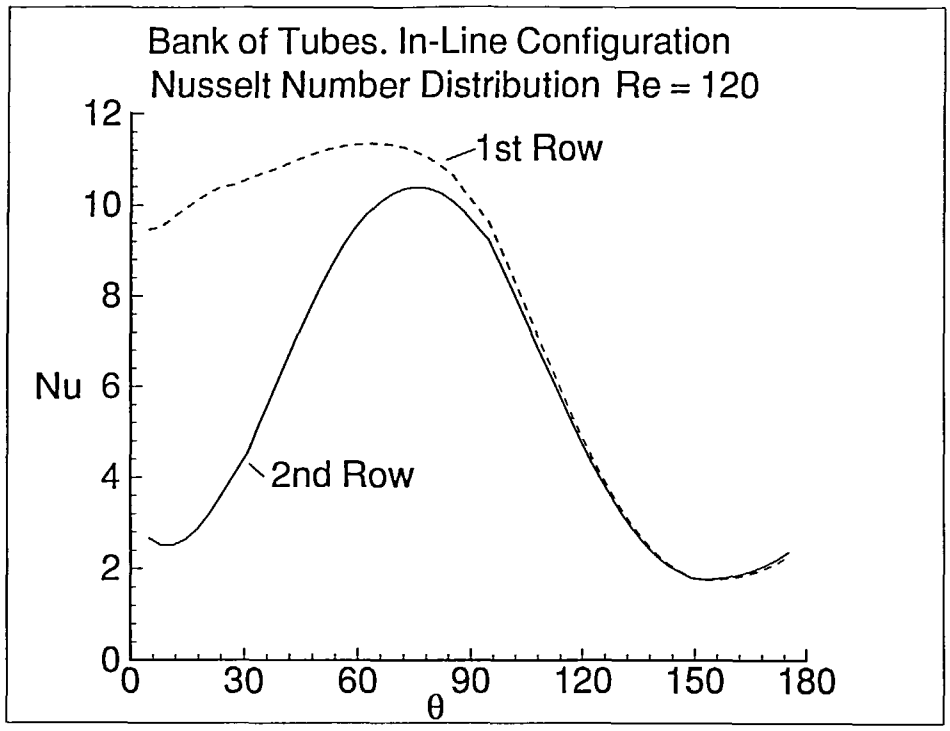

Figure 12

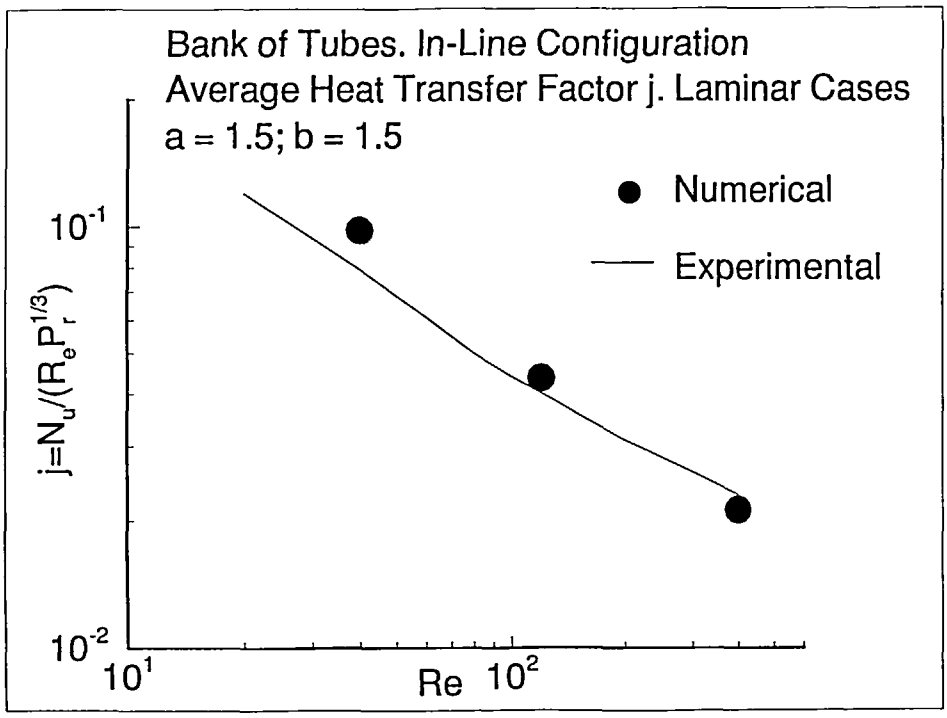

Figure 13

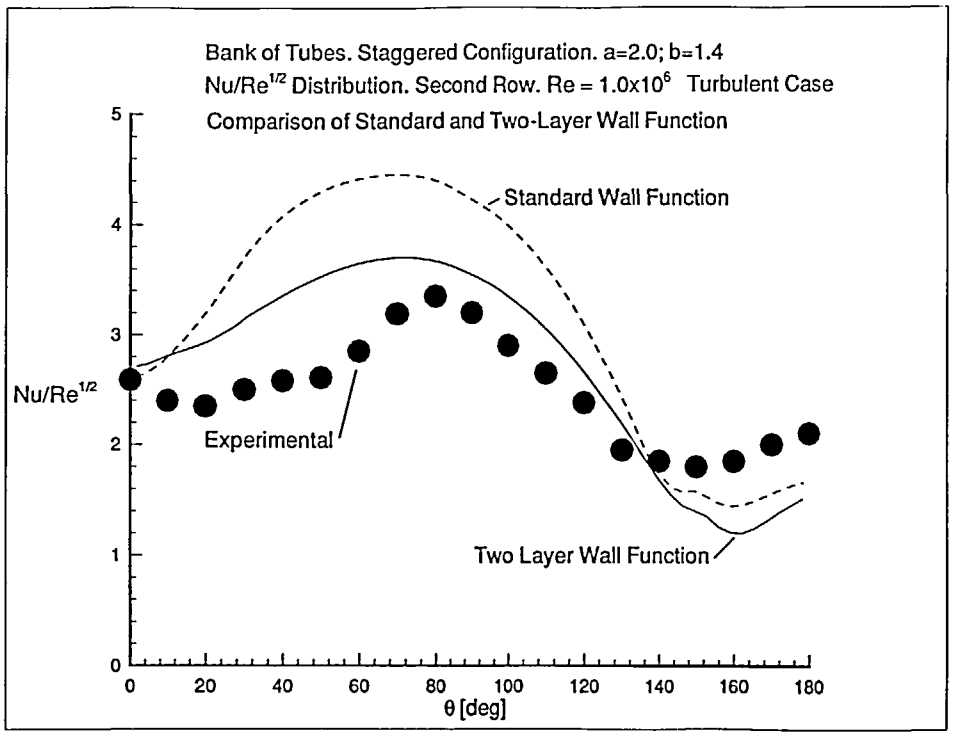

Figure 14

The difference between the use of a standard wall function and a two-layer wall function is also examined. A more accurate result is obtained with the two-layer wall function, indicating that the local heat transfer is very sensitive to the type of wall treatment used. Similar conclusions have been reported elsewhere[11]. It was also found that a finer and more dense grid is needed to obtain good agreement with experimental results for the local heat transfer distribution, because a good grid resolution is necessary close to the walls and also because the amount of grid stretching in the direction normal to the walls needs to be maintained at very low values ($1 + \varepsilon \leqslant 1.01$). The average Nusselt number for an in-line configuration with $a = 2.0$ and $b = 2.0$ in turbulent flow for different Reynolds numbers is presented in *Figure 15*, which agrees very well with experimental results[6].

Isotherms in a three-dimensional staggered configuration for turbulent flow are presented in *Figure 16*. In this case, hot air from the inlet (left) flows around the cold tubes and side walls, which are kept at constant temperature. The temperature drops faster in the regions of low speed flow (cylinder wake). The isotherms also show a temperature drop towards the side walls. The overall temperature patterns for this simulation are physically consistent.

CONCLUSIONS

A finite volume solution procedure has been used to predict complex laminar and turbulent flow and heat transfer through realistic tube bank geometries. The results have been validated for different tube bank configurations and flow regimes, and show very good agreement with available experimental data for two-dimensional cases, and are physically consistent for three dimensional cases. The validation of the local surface heat transfer results for different flow

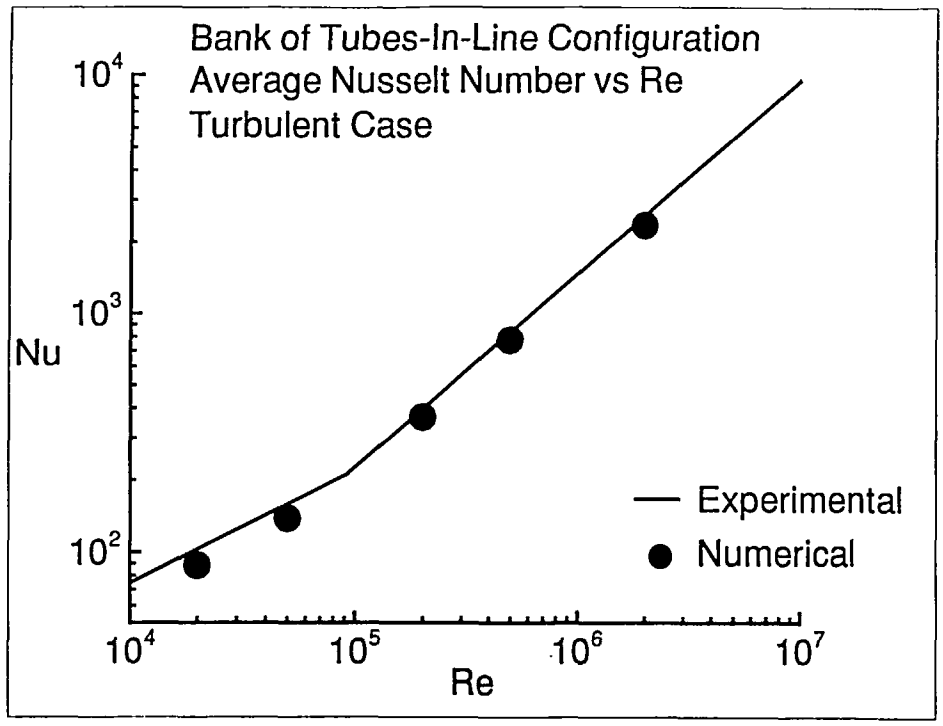

Figure 15

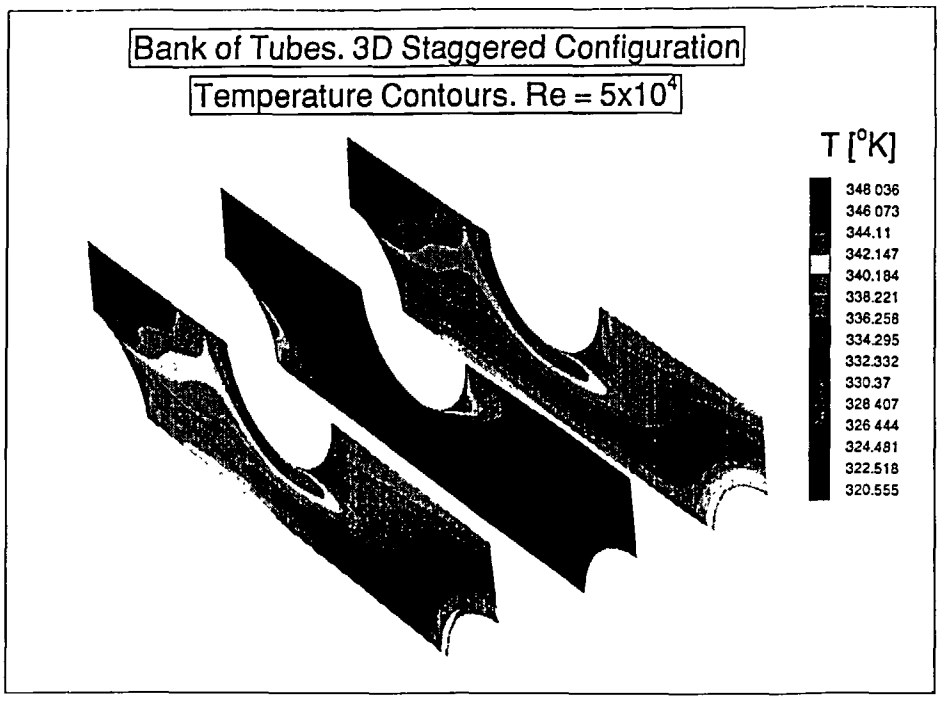

Figure 16

regimes has been carried to greater accuracy than in previous predictions, indicating that finer grids are required to be able to predict heat transfer accurately. The large number of flow conditions treated using the same numerical method provides a broad collection of test cases. The present algorithm has proven to be robust, computationally efficient and accurate, which makes it very attractive and reliable as a design tool for tube bank heat exchangers.

ACKNOWLEDGEMENTS

This research has been carried out as part of a DIST Generic Technology Project, 'Design Software for Power Utility Boilers', using equipment supplied, in part, by Pacific Power.

REFERENCES

1 Zhukauskas, A. and Ulinskas, R. *Heat Transfer in Tube Banks in Crossflow*, Springer-Verlag, Berlin (1988)
2 Fletcher, C. A. J. *Computational Techniques for Fluid Dynamics*, Vol. 1: *Fundamental and General Techniques*; Vol. 2: *Specific Techniques for Different Flow Categories*, Springer, Heidelberg (1991)
3 Launder, B. E. and Massey, T. H. The numerical prediction of viscous flow and heat transfer in tube banks, *J. Heat Transfer*, **100**, 565–571 (1978)
4 Fujii, M., Fujii, T. and Nagata, T. A numerical analysis of laminar flow and heat transfer of air in an in-line tube bank, *Num. Heat Transfer*, **7**, 89–102 (1984)
5 Nishimura, T., Itoh, H., Ohya, K. and Miyashita, H. Experimental validation of numerical analysis of flow across tube banks for laminar flow, *J. of Chemical Eng. of Japan*, **24**, No. 5, 666–669 (1991)
6 Antonopoulos, K. A. Heat transfer in tube banks under conditions of turbulent inclined flow, *Int. J. of Heat and Mass Transfer*, **28**, No. 9, 1645–1656 (1985)
7 Faghri, M. and Rao, N. Numerical computation of flow and heat transfer in finned and unfinned tube banks, *Int. J. of Heat and Mass Transfer*, **30**, No. 2, 363–372 (1987)
8 Launder, B. E. and Spalding, D. B. The numerical computation of turbulent flows, *Comp. Meth. in Applied Mech. and Eng.*, **3**, 263–289 (1974)
9 Gresho, P. M. Some current issues relevant to the incompressible Navier Stokes equations, *Minnesota Supercomputer Inst. Symp. on Recent Developments in Large-Scale C.F.D.* (1990)
10 Chieng, C. C. and Launder, B. E. On the calculation of turbulent heat transport downstream from an abrupt pipe expansion, *Num. Heat Transfer*, **3**, 189–207 (1980)
11 Djilali, N., Gartshore, I. and Salcudean, M. Calculation of convective heat transfer in recirculating turbulent flows using various near-wall turbulence models, *Num. Heat Transfer, Part A*, **16**, 189–212 (1989)
12 Fletcher, C. A. J. and Bain, J. G. An approximate factorisation explicit method for CFD, *Computers and Fluids*, **19**, 61–74 (1991)
13 Fletcher, C. A. J. Gas particle industrial flow simulation using RANSTAD, *Surveys in Fluid Mech.* (R. Narasinha, Ed.), **18**, 657–681 (1993)
14 Zdravistch, F. *Aerodynamic Flow Simulation Around Cluster Type Configurations*, Master's Thesis, ITA, Brazil (1990)
15 Gaddis, E. S. and Gnielinski, V. Pressure drop in cross flow across tube bundles, *Int. Chemical Eng.*, **25**, No. 1, 1–15 (1985)
16 Chang, Y., Beris, A. N. and Michaelides, E. E. A numerical study of heat and momentum transfer for tube bundles in crossflow, *Int. J. for Num. Meth. in Fluids*, **9**, 1381–1394 (1989)
17 Zhukauskas, A. Heat transfer from tubes in crossflow, *Advances in Heat Transfer*, **8**, 93–106 (1972)
18 Achenbach, E. Investigations on the flow through a staggered tube bundle at Reynolds numbers up to $Re = 10^7$, *Wäerme-und Stoffübertragung*, **2**, 47–52 (1969)
19 Bergelin, O. P., Brown, G. A. and Doberstein, S. C. Heat transfer and fluid friction during flow across banks of tubes – IV, *Trans. of the ASME*, **74**, 953–960 (1952)
20 Achenbach, E. Heat transfer from a staggered tube bundle in cross-flow at high Reynolds numbers, *Int. J. of Heat and Mass Transfer*, **32**, No. 2, 271–280 (1989)